





## Article

# Compressibility and Phase Stability of Iron-Rich Ankerite

Raquel Chuliá-Jordán <sup>1,\*</sup>, David Santamaria-Perez <sup>1</sup>, Javier Ruiz-Fuertes <sup>2</sup>, Alberto Otero-de-la-Roza <sup>3</sup>  
and Catalin Popescu <sup>4</sup>

<sup>1</sup> Departamento de Física Aplicada-ICMUV, Universitat de València, MALTA Consolider Team, 46100 Valencia, Spain; David.Santamaria@uv.es

<sup>2</sup> DCITIMAC, Universidad de Cantabria, MALTA Consolider Team, 39005 Santander, Spain; ruizfuertesj@unican.es

<sup>3</sup> Departamento de Química Física y Analítica, Facultad de Química, Universidad de Oviedo, MALTA Consolider Team, 33006 Oviedo, Spain; aoterodelaroz@gmail.com

<sup>4</sup> CELLS-ALBA Synchrotron Light Facility, Cerdanyola del Vallès, 08290 Barcelona, Spain; cpopescu@cells.es

\* Correspondence: Raquel.Chulia@uv.es

**Abstract:** The structure of the naturally occurring, iron-rich mineral  $\text{Ca}_{1.08(6)}\text{Mg}_{0.24(2)}\text{Fe}_{0.64(4)}\text{Mn}_{0.04(1)}(\text{CO}_3)_2$  ankerite was studied in a joint experimental and computational study. Synchrotron X-ray powder diffraction measurements up to 20 GPa were complemented by density functional theory calculations. The rhombohedral ankerite structure is stable under compression up to 12 GPa. A third-order Birch–Murnaghan equation of state yields  $V_0 = 328.2(3) \text{ \AA}^3$ , bulk modulus  $B_0 = 89(4) \text{ GPa}$ , and its first-pressure derivative  $B'_0 = 5.3(8)$ —values which are in good agreement with those obtained in our calculations for an ideal  $\text{CaFe}(\text{CO}_3)_2$  ankerite composition. At 12 GPa, the iron-rich ankerite structure undergoes a reversible phase transition that could be a consequence of increasingly non-hydrostatic conditions above 10 GPa. The high-pressure phase could not be characterized. DFT calculations were used to explore the relative stability of several potential high-pressure phases (dolomite-II-, dolomite-III- and dolomite-V-type structures), and suggest that the dolomite-V phase is the thermodynamically stable phase above 5 GPa. A novel high-pressure polymorph more stable than the dolomite-III-type phase for ideal  $\text{CaFe}(\text{CO}_3)_2$  ankerite was also proposed. This high-pressure phase consists of Fe and Ca atoms in sevenfold and ninefold coordination, respectively, while carbonate groups remain in a trigonal planar configuration. This phase could be a candidate structure for dense carbonates in other compositional systems.

**Keywords:** iron-rich ankerite; carbonate mineral; high pressure; phase transition; compressibility



check for updates

**Citation:** Chuliá-Jordán, R.; Santamaria-Perez, D.; Ruiz-Fuertes, J.; Otero-de-la-Roza, A.; Popescu, C. Compressibility and Phase Stability of Iron-Rich Ankerite. *Minerals* **2021**, *11*, 607. <https://doi.org/10.3390/min11060607>

Academic Editors: Anna Pakhomova and Ilya Kupenko

Received: 10 May 2021

Accepted: 2 June 2021

Published: 6 June 2021

**Publisher's Note:** MDPI stays neutral with regard to jurisdictional claims in published maps and institutional affiliations.



**Copyright:** © 2021 by the authors. Licensee MDPI, Basel, Switzerland. This article is an open access article distributed under the terms and conditions of the Creative Commons Attribution (CC BY) license (<https://creativecommons.org/licenses/by/4.0/>).

## 1. Introduction

The phase stability and elastic properties of minerals depend essentially on three intrinsic variables: the chemical composition ( $X$ ), the pressure ( $P$ ), and the temperature ( $T$ ) [1,2]. The actual crystal structure of a mineral also depends on the associated energy landscape, which indicates the possible existence of the local minima, activation barriers, kinetic effects, and metastable phases [3,4]. Understanding the formation processes and stability of carbonate minerals under different thermodynamic conditions is crucial for Earth sciences and the geological carbon cycle. Carbonates are important components of the Earth's surface, and are continuously incorporated into the mantle via subduction. In the mantle, carbonates may decompose, reduce, or survive depending on the aforementioned variables [5]. Previous studies have demonstrated that carbonates of divalent metals with different radii and electronic characteristics present distinctive behaviors under compression and heating [6–10]. This is particularly relevant within the complex scenario of Earth's mantle, where natural compositions likely include the coexistence of several divalent cations.

The structural behavior and physical properties of pure  $\text{CaMg}(\text{CO}_3)_2$  dolomite and iron-bearing dolomite  $\text{CaMg}_x\text{Fe}_{1-x}(\text{CO}_3)_2$  compositions have been studied at high pressures

and/or high temperatures [11–22]. The structure of  $\text{CaMg}(\text{CO}_3)_2$  dolomite is rhombohedral (space group  $R\bar{3}$ ) at ambient conditions, and can be described as a combination of alternating calcite- and magnesite-like layers [23,24]. In naturally occurring iron-rich dolomites (named ankerites), about half of the Mg atoms are substituted by Fe atoms, although a small amount of manganese is usually present. The pure iron analogue of dolomite,  $\text{CaFe}(\text{CO}_3)_2$ , has never been synthesized or found in nature [25]. High-pressure, ambient-temperature structural studies on iron-bearing dolomite with stoichiometry  $\text{CaMg}_{0.6}\text{Fe}_{0.4}(\text{CO}_3)_2$  revealed two phase transitions at 17 and 35 GPa [11,19]. The novel high-pressure polymorphs, named dolomite-II and -III, are triclinic, and the coordination number of their cations increases from 6 at ambient pressure to 7/8 and 7/9, respectively. Dolomite-III features a 3 plus 1 carbon coordination at 60 GPa [19]. Moreover, a recent theoretical DFT study of dolomite predicted a low-energy monoclinic  $C2/c$  polymorph above 15 GPa, whose thermodynamic stability would increase with iron content [12,14]. This phase was subsequently found in high-pressure (between 40 and 60 GPa) and high-temperature (1800–2300 K) experiments, remaining stable down to 12 GPa at ambient temperature. All of these phases could play important roles as carbon carriers in the Earth's mantle cycling [11,19].

The structural behavior of a ferroan dolomite with higher Fe content upon compression was reported in [10]. Single-crystal X-ray diffraction (XRD) measurements of the  $\text{CaMg}_{0.27}\text{Fe}_{0.68}\text{Mn}_{0.05}(\text{CO}_3)_2$  carbonate were performed up to 4 GPa, and no phase transitions were observed in the studied pressure range. The isothermal bulk modulus and axial compressibilities were determined, and the results showed that the  $\text{Mg} \leftrightarrow \text{Fe}$  substitution does not cause noticeable changes in the compressional parameters.

In this work, we have carried out in situ powder XRD measurements at pressures up to 20 GPa on the naturally occurring iron-rich  $\text{Ca}_{1.08(6)}\text{Mg}_{0.24(2)}\text{Fe}_{0.64(4)}\text{Mn}_{0.04(1)}(\text{CO}_3)_2$  ankerite, similar in composition to that studied by Ross et al. [10]. We found that ankerite undergoes a phase transition above 12 GPa to a polymorph not previously reported in literature. Our P–V data are compared to those from other dolomite experiments, and the effect of Mg–Fe substitution on dolomite carbonates is discussed. DFT calculations on the hypothetical pure  $\text{CaFe}(\text{CO}_3)_2$  ankerite shed light on its phase stability and complement the experimental results.

## 2. Materials and Methods

### 2.1. Experimental Details

Naturally occurring ankerite crystals from Erzberg (Austria) were kindly provided by the Yale Peabody Museum (Specimen YPM MIN 032451). Some of the crystals were crushed to obtain a fine white powder. Quantitative chemical analyses were performed with a Philips XL30 scanning electron microscope using energy-dispersive X-ray spectroscopy. According to these analyses, the chemical composition of our ankerite sample was  $\text{Ca}_{1.08(6)}\text{Mg}_{0.24(2)}\text{Fe}_{0.64(4)}\text{Mn}_{0.04(1)}(\text{CO}_3)_2$ . Powder XRD data at ambient conditions confirmed the dolomite-type structure.

High-pressure angle-dispersive powder XRD experiments were conducted at the MSPD beamline of the ALBA-CELLS synchrotron light source [26] located in Cerdanyola del Vallès (Spain), using a monochromatic incident beam of 0.4246 Å. HP measurements were performed using a diamond anvil cell (DAC)—a technique that allowed us to strongly modify the atomic interactions and characterize in situ the samples [27,28]. In our room-temperature high-pressure (HP) experiment, the ankerite sample was placed in a stainless steel gasket cavity inside the gas-membrane-driven DAC, together with Cu powder used for pressure determination [29], and a 4:1 mixture of methanol–ethanol used as a pressure-transmitting medium [30]. Diffraction patterns were collected at different pressures for 20 s up to 20 GPa at room temperature.  $\text{LaB}_6$  powder was used for distortion correction, and integration to conventional  $2\theta$ -intensity data was carried out using Dioptas software version 0.5.0 [31]. The indexing and refinement of the powder patterns were performed using the UnitCell [32] and PowderCell [33] program packages.

## 2.2. Computational Details

The equations of state (EOSs) and structural parameters of the five phases (ankerite, HP-ankerite, dolomite-II, dolomite-III and dolomite-V) were calculated using density functional theory (DFT) under periodic boundary conditions. We used the plane-wave approach in the projector-augmented wave (PAW) formalism [34], as implemented in Quantum ESPRESSO [35] version 6.5. The PAW datasets for Ca (8 valence electrons), C (4), and Fe (16) were obtained from PSlibrary version 1.0 [36]. We used the PBEsol exchange correlation functional [37]. We expected the magnetic behavior of the three phases to be similar under pressure, so we made some simplifications to our computational procedure. First, in all cases, we considered only the ferromagnetic ordering. This greatly improved the stability of the self-consistent field (SCF) procedure in our calculations, allowing us to use the primitive unit cell, and circumventing the need to consider various atomic magnetic moment permutations for each phase, as would be the case had we used an antiferromagnetic ordering. We did not use a Hubbard-like or a similar correction to the d orbitals of Fe because of problems with the SCF convergence and the smoothness of the resulting equations of state. In addition, no magnetic transitions were observed in the studied pressure range.

The cutoff energies for the wave function and density plane-wave expansions were 100 Ry and 1000 Ry, respectively. Shifted uniform (Monkhorst–Pack) k-point grids were used with  $6 \times 6 \times 6$  (ankerite),  $4 \times 4 \times 2$  (HP-ankerite),  $4 \times 4 \times 4$  (dolomite-II),  $3 \times 2 \times 2$  (dolomite-III), and  $4 \times 4 \times 4$  (dolomite-V) k-points. These parameters yield less than 0.1 mRy in the total energy, and less than 0.01 GPa in the calculated pressure. Smearing of the Kohn–Sham state occupations was applied using Marzari–Vanderbilt (cold) smearing [38], with a smearing parameter of 0.001 Ry.

Geometry relaxations were carried out for each phase at zero pressure and 50 GPa. The optimization used tight total energy and force convergence thresholds ( $10^{-5}$  Ry in the energy and  $10^{-4}$  Ry/bohr in the forces). Next, a volume grid was constructed with 41 points between the 0 and 50 GPa volumes. Subsequent fixed-volume geometry relaxation yielded the EOS for each phase. The Gibbs2 program [39,40] was used to calculate the enthalpy vs. pressure and energy vs. volume diagrams, as well as the phase transition sequence, from the EOS data.

## 3. Results and Discussion

Before studying our ankerite sample under compression we performed an ambient-conditions powder XRD measurement to confirm its structure. The indexation of our data confirmed a rhombohedral symmetry with lattice parameters  $a = 4.8361(9)$  Å and  $c = 16.185(3)$  Å ( $V = 327.83(1)$  Å<sup>3</sup>), in excellent agreement with those expected from the Goldsmith linear regression formulae interrelating chemical composition and hexagonal lattice constants ( $a = 4.834$  Å and  $c = 16.185$  Å) [41], and those from previous studies on iron-rich ankerites [10,24]. The Rietveld refinement of the ambient-conditions powder XRD pattern suggests the following values for refinable atomic coordinates:  $z_C = 0.244(2)$ ,  $x_O = 0.919(2)$ ,  $y_O = 0.302(4)$ , and  $z_O = 0.576(2)$ , in agreement with our calculated values ( $z_C = 0.2428$ ,  $x_O = 0.9206$ ,  $y_O = 0.3084$ , and  $z_O = 0.5770$ ) and results from other literature [10]. The crystal structure of ankerite, depicted in Figure 1, is similar to that of dolomite. Like calcite, it consists of alternating layers of cations and [CO<sub>3</sub>] carbonate groups, which adopt a highly deformed NaCl (B1) structure type [23]. The diagonal of the B1 structure is shortened in order to properly accommodate the carbonate groups. However, in dolomite and ankerite, different cations are present, and Ca and Mg/Fe cations are segregated in alternate layers. In our case, the ankerite stoichiometry has an 8% Ca mole fraction in the Fe/Mg layers. The accommodation of metal atoms of different sizes entails a small rotation of the CO<sub>3</sub> groups of each layer around the threefold axis with respect to their position in calcite (space group  $R\bar{3}c$ ), which means that these groups cannot be related by a  $c$ -glide.

Once the crystal structure of ankerite was confirmed at ambient conditions, we studied it under compression at room temperature. Synchrotron XRD measurements showed that

the initial rhombohedral phase was stable up to 12 GPa (Figure 2). Under compression, all of the diffraction peaks shifted to higher angles, as expected for a decrease in interplanar distances. Above 4 GPa, a new diffraction peak appeared in the CCD image, marked with an asterisk in the integrated XRD pattern at 9.5 GPa in Figure 2. This peak corresponds to the (210) reflection of the molecular CO<sub>2</sub>-I solid phase, as inferred from the indexed volumes and its equation of state [42]. As far as we know, the formation of carbon dioxide in a room-temperature compression experiment on a carbonate has never been reported, with the decomposition process requiring high temperatures. We speculate that the Cu metal used as an internal pressure gauge could have catalyzed this process. No other additional Bragg peaks were observed in the 0–12 GPa pressure range, so we could study the evolution of the iron-rich ankerite structure under compression. Unfortunately, the XRD patterns present texturing effects due to uneven crystal sizes, precluding full structural refinements. Lattice parameters and unit cell volumes at different pressures from Le Bail refinements are collected in Table 1.

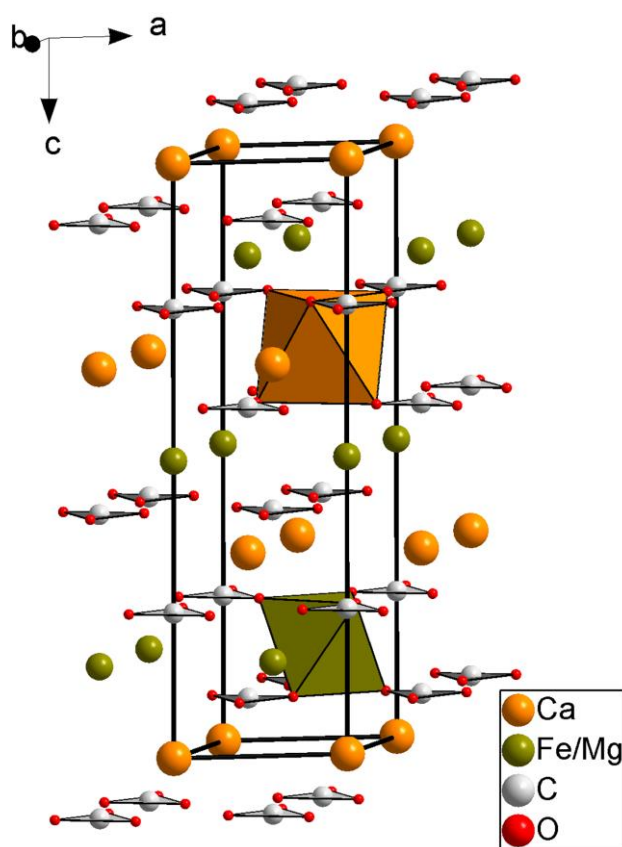


**Figure 1.** Iron-rich  $R\bar{3}$  ankerite structure under ambient conditions. Triangular [CO<sub>3</sub>], and octahedral (CaO<sub>6</sub>) and ((Fe/Mg)O<sub>6</sub>) units are colored light gray, orange, and green, respectively, as with the central atoms. The O atoms are colored in red. The unit cell is depicted by a solid black line.

The evolution of the unit-cell volumes of our Ca<sub>1.08(6)</sub>Mg<sub>0.24(2)</sub>Fe<sub>0.64(4)</sub>Mn<sub>0.04(1)</sub>(CO<sub>3</sub>)<sub>2</sub> iron-rich ankerite upon compression at room temperature is plotted in Figure 3, where we compare them with previous experimental data up to 4 GPa and those obtained in our theoretical calculations. The pressure–volume curves were analyzed using a third-order Birch–Murnaghan (BM) equation of state (EOS) [43]. The fitting of our experimental values yields a zero-pressure volume  $V_0 = 328.9(5) \text{ \AA}^3$ , a bulk modulus  $B_0 = 83(6) \text{ GPa}$ , and its first-pressure derivative  $B'_0 = 6.2(11)$ ; and  $V_0 = 328.0(2) \text{ \AA}^3$  and  $B_0 = 94.7(11) \text{ GPa}$  when fixing the  $B'_0$  to 4. These results compare well with the compressibility of a compositionally similar ankerite reported by Ross and Reeder using a second-order BM EOS ( $V_0 = 327.82(11) \text{ \AA}^3$  and  $B_0 = 91.7(4) \text{ GPa}$ ) [10]. Taking into account both our and

previous [10] datasets, the EOS fit to all of the experimental high-pressure P–V values yields  $V_0 = 328.2(3) \text{ \AA}^3$ , a bulk modulus  $B_0 = 89(4) \text{ GPa}$ , and its first-pressure derivative  $B'_0 = 5.3(8)$ . In the case of the calculations for pure  $\text{FeCa}(\text{CO}_3)_2$ , the obtained values for  $V_0$ ,  $B_0$ , and  $B'_0$  are  $319.29(6) \text{ \AA}^3$ ,  $99.4(7) \text{ GPa}$ , and  $3.85(8)$ , respectively. Note that the experimental compressibility is in good agreement with that predicted by our ab initio calculations. Our results show that the bulk moduli of our ferroan dolomite and the pure  $\text{CaMg}(\text{CO}_3)_2$  dolomite ( $B_0 = 94.1(7) \text{ GPa}$  and  $B'_0$  fixed to 4 [10]) are similar. This is consistent with the fact that carbonate ( $\text{CO}_3$ ) units are incompressible, rigid units, and the overall compression of the structure is due to the cation-centered ( $\text{CaO}_6$ ) and  $((\text{Fe,Mg})\text{O}_6)$  octahedra. The latter of these motifs has similar compressibility regardless of whether it is occupied by Fe or Mg atoms. We can also compare the observed compressibility with that of related calcite-type carbonates ( $B_{0,\text{CaCO}_3} = 67(2) \text{ GPa}$ ,  $B_{0,\text{FeCO}_3} = 117(1) \text{ GPa}$ ,  $B_{0,\text{MgCO}_3} = 107(1) \text{ GPa}$ ,  $B_{0,\text{MnCO}_3} = 107(1) \text{ GPa}$ ) [6], and conclude that the bulk modulus of iron-rich ankerites is approximately the mean of the bulk moduli of the two end-member carbonates with major cation proportions in each layer:  $B_0(\text{Ca}_x(\text{Fe,Mg})_{1-x}\text{CO}_3) \sim (B_0(\text{CaCO}_3) + B_0(\text{FeCO}_3))/2 = (67(2) + 117(1))/2 = 92(2) \text{ GPa}$ .

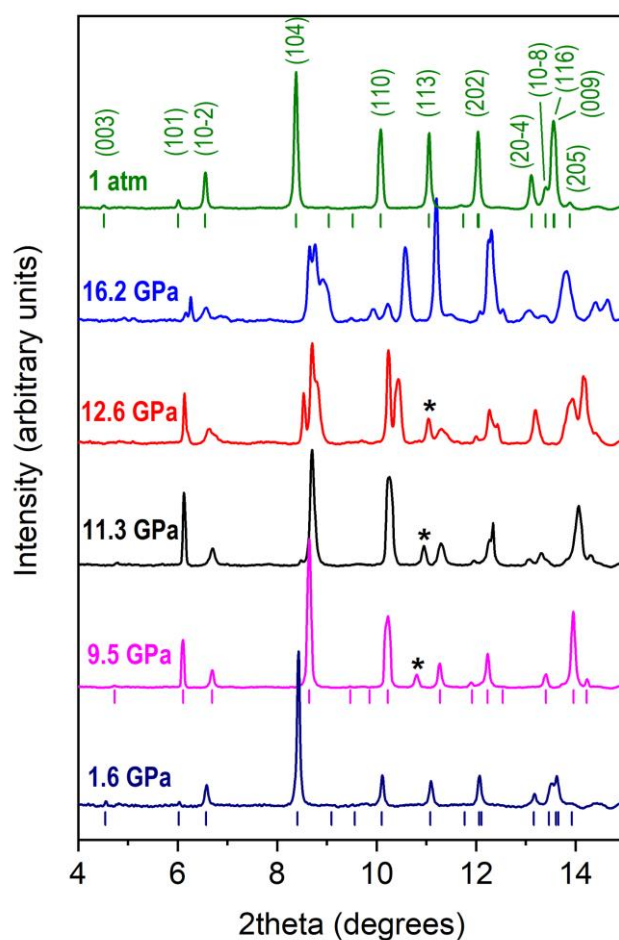


**Figure 2.** Selected powder XRD patterns of  $\text{Ca}_{1.08(6)}\text{Mg}_{0.24(2)}\text{Fe}_{0.64(4)}\text{Mn}_{0.04(1)}(\text{CO}_3)_2$  ankerite from experiments. Backgrounds have been subtracted. Reflections of the initial dolomite-type structure are indicated as vertical marks and labelled. The diffraction peak assigned to the (210) reflection of the molecular  $\text{CO}_2$ -I solid phase is denoted with an asterisk (\*). Synchrotron radiation wavelength was  $0.4246 \text{ \AA}$ .

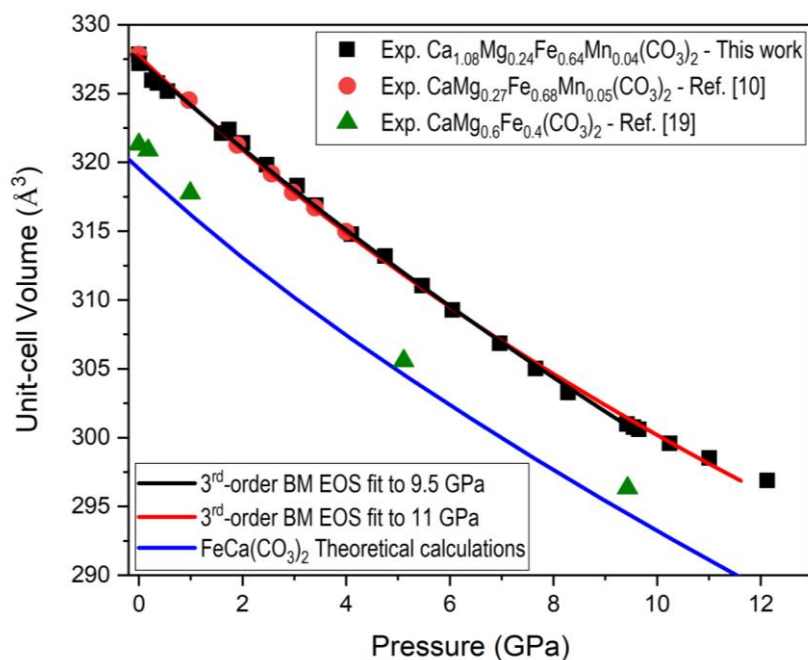


**Table 1.** Experimentally determined lattice parameters ( $a$  and  $c$ ) and unit cell volume of  $R\bar{3}Ca_{1.08(6)}Mg_{0.24(2)}Fe_{0.64(4)}Mn_{0.04(1)}(CO_3)_2$  ankerite at different pressures. Pressure uncertainties are estimated to be  $\sim 0.05$  GPa below 8 GPa, and  $\sim 0.1$  GPa above this pressure.

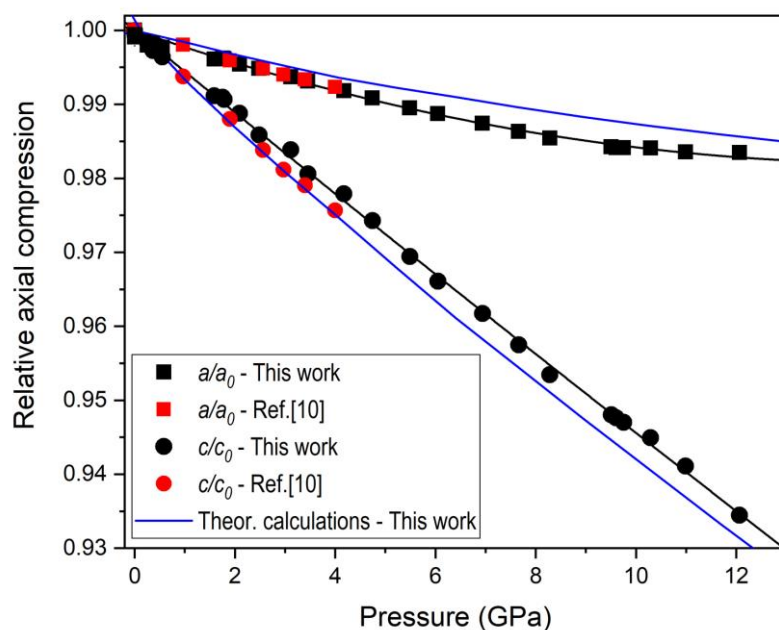
Pressure (GPa)	$a$ Axis (Å)	$c$ Axis (Å)	Unit Cell Volume (Å <sup>3</sup> )
0.00	4.8361(12)	16.185(7)	327.83(15)
0.01	4.8262(12)	16.174(7)	327.18(15)
0.26	4.8273(11)	16.160(7)	325.96(14)
0.36	4.8361(11)	16.142(7)	325.75(14)
0.56	4.8249(11)	16.128(7)	325.15(14)
1.60	4.8171(14)	16.043(13)	322.39(19)
1.75	4.8177(14)	16.040(13)	322.40(19)
1.80	4.8173(14)	16.035(13)	322.26(19)
2.10	4.8137(14)	16.004(13)	321.17(19)
2.50	4.8111(14)	15.957(12)	319.86(19)
3.10	4.8054(14)	15.925(12)	318.47(19)
3.45	4.8028(14)	15.872(12)	317.07(19)
4.20	4.7964(13)	15.828(12)	315.35(18)
4.75	4.7917(13)	15.769(12)	313.56(18)
5.50	4.7851(13)	15.691(12)	311.15(18)
6.05	4.7815(13)	15.637(12)	309.61(18)
6.95	4.7751(13)	15.566(11)	307.39(18)
7.65	4.7698(13)	15.498(11)	305.35(17)
8.3	4.7654(13)	15.432(11)	303.50(17)
9.5	4.7598(13)	15.345(11)	301.07(17)
9.6	4.7592(13)	15.338(11)	300.86(17)
9.8	4.7591(13)	15.328(11)	300.66(17)
10.3	4.7590(13)	15.294(11)	299.98(17)
11.0	4.7565(13)	15.232(11)	298.45(17)
12.1	4.7560(14)	15.125(11)	296.28(17)

We mentioned above that ankerite has the  $(CO_3)$  units arranged in layers and oriented perpendicular to the  $c$  axis, and that these carbonate groups share corners with interlayer cation  $((Ca,Fe,Mg)O_6)$  octahedra. This spatial arrangement explains the experimentally observed axial compressibilities. Figure 4 illustrates the evolution of the  $a/a_0$  and  $c/c_0$  lattice parameter ratios with increasing pressure, which suggests that their contraction is rather anisotropic. According to our experiments, the compressibility of the  $a$  axis is considerably less than that of the corresponding  $c$  axis. Experimental (calculated) axial linear compressibilities for ankerite in the 0–9 GPa range, defined as  $\beta_x = (-1/x)(\partial x/\partial P)$ , are  $\beta_a = 1.66(2) \times 10^{-3}$  ( $1.25(5) \times 10^{-3}$ ) and  $\beta_c = 5.64(5) \times 10^{-3}$  ( $5.77(9) \times 10^{-3}$ )  $GPa^{-1}$ . The calculated  $\beta_c$  is in good agreement with the experimental values, but the predicted  $\beta_a$  is significantly smaller than the experimental value. According to the experiments, the  $\beta_c/\beta_a$  axial compression ratio is 3.40(6), and the  $c/a$  axes ratio increases with pressure according to the expression  $c/a = 3.353(1) - 0.0136(2) \times P$ . The slope of this straight line is similar to that obtained by Ross and Reeder [10], as well as our DFT calculations (Figure 5). This anisotropic lattice behavior is due to the fact that the C–O bonds, which are arranged parallel to the  $ab$  plane, are much less compressible than the Ca/Fe/Mg–O bonds. Thus, from our calculations, we observed that the interatomic Ca–O and Fe–O distances

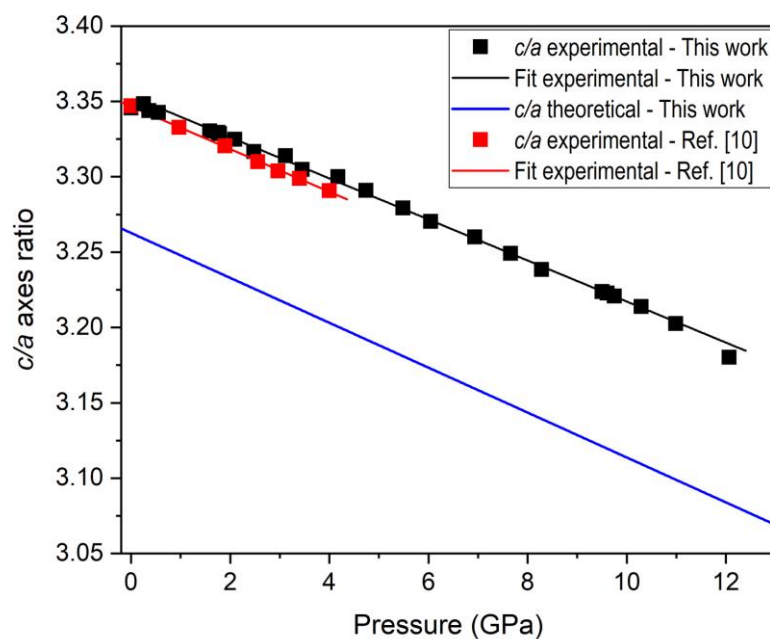
shortened by  $\sim 3.22\%$  and  $2.88\%$ , respectively, between atmospheric pressure and 10 GPa, whereas the C–O distance only varied  $0.54\%$  in the same pressure range.



**Figure 3.** Pressure–volume data per unit cell. Black squares, red circles, and green triangles refer to our  $\text{Ca}_{1.08(6)}\text{Mg}_{0.24(2)}\text{Fe}_{0.64(4)}\text{Mn}_{0.04(1)}(\text{CO}_3)_2$  experimental (Exp.) data and the reported data by Ross and Reeder ( $\text{CaMg}_{0.27}\text{Fe}_{0.68}\text{Mn}_{0.05}(\text{CO}_3)_2$ ) [10] and Merlini et al. ( $\text{CaMg}_{0.6}\text{Fe}_{0.4}(\text{CO}_3)_2$ ) [19], respectively. The black and red lines represent the fits of our room-temperature experimental data with a third-order Birch–Murnaghan EOS in the quasi-hydrostatic pressure range and up to 11 GPa, to be compared with the theoretically calculated  $P$ – $V$  curve for pure  $\text{CaFe}(\text{CO}_3)_2$  ankerite (blue line).



**Figure 4.** Relative axial compressibilities of the iron-rich ankerite structure. Experimental relative contractions  $a/a_0$  and  $c/c_0$  are represented as solid squares and circles, respectively (black: our data; red: data from [10]). Results from DFT calculations for pure  $\text{CaFe}(\text{CO}_3)_2$  ankerite are depicted as blue lines.



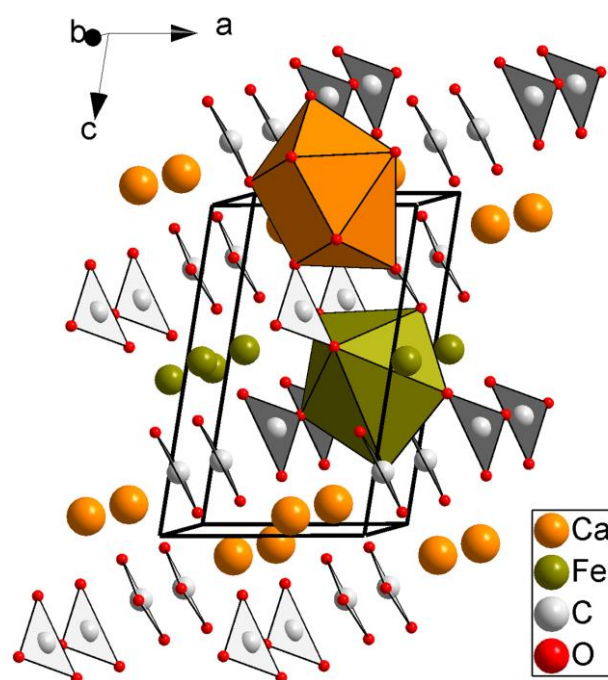
**Figure 5.**  $c/a$  axes ratio as a function of pressure. Black squares and red circles refer to our  $\text{Ca}_{1.08(6)}\text{Mg}_{0.24(2)}\text{Fe}_{0.64(4)}\text{Mn}_{0.04(1)}(\text{CO}_3)_2$  experimental data and the reported data by Ross and Reeder [10], respectively. Results from DFT calculations for pure  $\text{CaFe}(\text{CO}_3)_2$  ankerite are represented as a blue line.

Figure 4 shows that the compressibility of the  $a$  axis significantly decreases above 9 GPa, which could be caused by deviatoric stresses as a consequence of the loss of hydrostaticity of the methanol–ethanol pressure-transmitting medium [30]. At pressures higher than 12.6 GPa, additional diffraction peaks progressively appear (Figure 2). We tried to index the XRD pattern above that pressure, assuming the possibility of phase coexistence between the low-pressure  $R\bar{3}$  phase and a new high-pressure (HP) phase, or assuming a single HP phase. Major decomposition or chemical reaction processes were ruled out, because the initial rhombohedral ankerite structure was recovered after decompression (Figure 2). As potential HP structures we considered the two dense polymorphs (-II and -III) found for both  $\text{CaMg}_{0.92}\text{Fe}_{0.08}(\text{CO}_3)_2$  dolomite [44] and a more Fe-enriched dolomite  $\text{CaMg}_{0.6}\text{Fe}_{0.4}(\text{CO}_3)_2$  [19], above 17 and 35 GPa, respectively. We also considered the recently reported HP–HT polymorph-V [12,14,21]. However, these structures did not allow us to explain the new peaks. We then proceeded to use our best indexing at 16.2 GPa to try to elucidate the HP phase by means of the Endeavour software [45]. The indexed lattice parameters at this pressure were  $a = 5.274(7)$  Å,  $b = 4.148(4)$  Å,  $c = 9.261(11)$  Å,  $\alpha = 78.99(9)^\circ$ ,  $\beta = 111.35(8)^\circ$ , and  $\gamma = 107.02(9)^\circ$  ( $M$  (9 peaks) = 37.8, and  $V = 179.6$  Å<sup>3</sup> for the assumed 2 formula units in the unit cell). This unit cell would entail a volume collapse of approximately 6% at the transition. The structure solution was performed using a special variant of the “direct space” approach—namely, a combined global optimization of the difference between the calculated and observed diffraction data, and of the potential energy of the system. Due to the usage of the potential energy, this method has been used to solve several HP novel crystalline phases [46,47]. The Endeavour program suggested a potential structure that was subsequently relaxed using DFT calculations. The calculated final structure, however, could not explain the experimental XRD pattern either, but it resulted in a thermodynamically competitive phase at high pressures for an ideal  $\text{CaFe}(\text{CO}_3)_2$  ankerite composition. The lattice parameters and atomic coordinates of the substance hereafter called “HP-ankerite” are shown in Table 2, and the structure is depicted in Figure 6.



**Table 2.** Calculated atomic coordinates for the  $P\bar{1}$  “HP-ankerite” phase at 35.2 GPa. The lattice parameters at this pressure would be:  $a = 4.985 \text{ \AA}$ ,  $b = 4.136 \text{ \AA}$ ,  $c = 8.250 \text{ \AA}$ ,  $\alpha = 76.11^\circ$ ,  $\beta = 99.13^\circ$ , and  $\gamma = 105.82^\circ$ .

Atom	Atomic Coordinates		
	$x$	$y$	$z$
Ca	0.3086	0.6672	0.0719
Fe	0.1347	0.3180	0.4615
C	0.5655	0.2320	0.3151
C	0.0567	0.0757	0.8053
O	0.0511	0.7440	0.3225
O	0.2078	0.2069	0.9225
O	0.9949	0.2440	0.1855
O	0.7198	0.0792	0.4260
O	0.4813	0.1549	0.1745
O	0.5023	0.4917	0.3469



**Figure 6.** Structure of the calculated  $P\bar{1}$  “HP-ankerite” phase for pure  $\text{CaFe}(\text{CO}_3)_2$  ankerite at 35.2 GPa. The red spheres represent the O atoms, whereas the light gray, orange, and green spheres correspond to C, Ca, and Fe atoms, respectively. The  $(\text{CaO}_9)$  and  $(\text{FeO}_7)$  polyhedra are also depicted.

In order to get further insight into the relative thermodynamic stability of the different possible  $\text{CaFe}(\text{CO}_3)_2$  polymorphs and their pressure-induced transformations, we have performed ab initio total-energy calculations of our “HP-ankerite” phase, the low-pressure dolomite-type ankerite [10], and the high-pressure dolomite-II- [11,19], dolomite-III- [19], and dolomite-V-type phases [12,14,21]. The aim was to check the stability of this suggested phase with respect to other experimentally observed phases in iron-containing dolomites that could be candidates for high-pressure phases of pure ankerite.

Figure 7 shows the calculated curves for energy as a function of volume, and the enthalpies calculated for each phase referring to the enthalpy of dolomite-type pure ankerite are shown in the inset. According to our calculations, the enthalpies of the dolomite- and

dolomite-II-type phases are very similar below 15 GPa (within 0.04 eV per formula unit of one another), the dolomite-II-type enthalpy curve lying below that of dolomite. Therefore, the dolomite-II-type phase would be the most thermodynamically stable phase amongst those considered, and the small energy difference between the dolomite- and dolomite-II-type phases could indicate that either of them may be observable under the proper experimental conditions for  $\text{CaFe}(\text{CO}_3)_2$  ankerite. It should be noted that the relaxation of the dolomite-II phase converges to a structure similar to that of the dolomite-type ankerite at pressures below 18 GPa, with Ca and Fe atoms being octahedrally coordinated. Only above this pressure, the coordination of the Ca atoms increases to 7 in the dolomite-II phase. The plot of the theoretical enthalpy also indicates that, above 31 GPa, the “HP-ankerite” phase reported here for the first time for  $\text{CaFe}(\text{CO}_3)_2$  is energetically more stable than the dolomite-III-type phase found experimentally at high pressures in iron-bearing dolomite. Nevertheless, as shown in Figure 7, our DFT calculations confirm the results of previous theoretical studies [12,14], which predicted that the  $C2/c$  dolomite-V phase is the thermodynamically stable phase above 5 GPa. This phase has only been observed experimentally after heating.

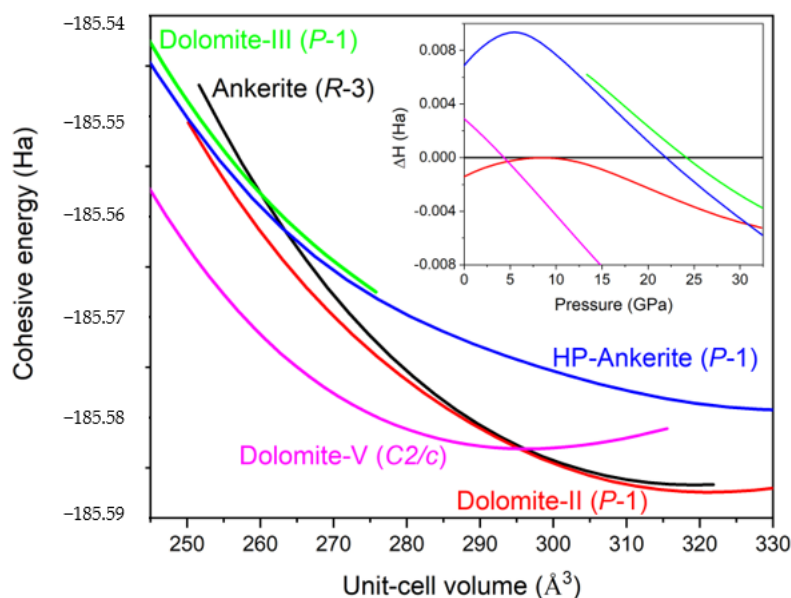


**Figure 7.** Cohesive energy as a function of the volume per  $\text{CaFe}(\text{CO}_3)_2$  formula unit for the  $R\bar{3}$  dolomite-I-type,  $P\bar{1}$  dolomite-II-type [19],  $P\bar{1}$  dolomite-III-type [19],  $C2/c$  dolomite-V-type [12], and the  $P\bar{1}$  “HP-ankerite” (this work) ankerite phases. Inset: Enthalpy difference as a function of pressure, showing the stabilities with respect to  $R\bar{3}$   $\text{CaFe}(\text{CO}_3)_2$  ankerite.

The “HP-ankerite” phase is depicted in Figure 6. It consists of trigonal planar ( $\text{CO}_3$ ) carbonate groups, ( $\text{FeO}_7$ ) pentagonal bipyramids, and complex ( $\text{CaO}_9$ ) polyhedra. This structure presents an increase in the coordination number of the Ca atoms from the dolomite-II-type phase, where the Fe and Ca atoms are six- and sevenfold coordinated by oxygen atoms, respectively. The carbonate groups are no longer parallel between them, like in ankerite or the dolomite-II phase, but they adopt two different orientations. The structure is so different that it could not be considered a simple distortion of the low-pressure phases. Note that ninefold or higher coordination for Ca atoms has been found in other carbonate phases, such as  $\text{CaCO}_3$  aragonite [48], dense  $\text{BaCa}(\text{CO}_3)_2$  alstonite [9,49], and calcium silicate-carbonates [50,51]. The irregular and large cation-centered oxygen polyhedra of this potential ankerite HP phase suggest that other divalent cation species could be accommodated in these sites. Therefore, this phase is a candidate for dense carbonate structures in other compositional systems.

#### 4. Conclusions

Iron-bearing carbonates are candidate phases for carbon storage in deep Earth, and may play an important role in the geological carbon cycle. Subducting slabs, for instance, likely carry iron-bearing carbonates to the mantle, where high-pressure, high-temperature conditions modify their physical properties. In this study we tried to elucidate the structural behavior of (1) natural iron-rich  $\text{Ca}_{1.08(6)}\text{Mg}_{0.24(2)}\text{Fe}_{0.64(4)}\text{Mn}_{0.04(1)}(\text{CO}_3)_2$  ankerite under compression using synchrotron X-ray diffraction, and (2) ideal pure  $\text{CaFe}(\text{CO}_3)_2$  ankerite using DFT calculations. The latter stoichiometric composition of ankerite has never been found to occur naturally, nor synthesized in a laboratory as an ordered phase. To date, only a disordered structure has been achieved, but thermodynamic models predict the stability of ordered  $\text{CaFe}(\text{CO}_3)_2$  ankerite below 450 °C [25].

Our experiments on natural  $\text{Ca}_{1.08(6)}\text{Mg}_{0.24(2)}\text{Fe}_{0.64(4)}\text{Mn}_{0.04(1)}(\text{CO}_3)_2$  ankerite reveal that the initial rhombohedral dolomite-type structure is stable up to 12 GPa, where it undergoes a phase transition. Unfortunately, the structure of the high-pressure polymorph could not be identified, but the recovery of the initial structure indicates its reversible character, and rules out chemical reactions or significant decomposition. In order to shed light on the high-pressure phase diagram of this iron-rich carbonate, we undertake a DFT study of the stability of different candidate phases for a pure  $\text{CaFe}(\text{CO}_3)_2$  composition. Previous experimentally observed polymorphs of dense dolomite were considered [11,19], as well as a tentative structure named “HP-ankerite” suggested by the indexation of the high-pressure powder pattern and potential energy calculations. Ab initio calculations show that, above 31 GPa, this latter high-pressure phase is more stable than the experimentally observed dolomite-III phase, but the dolomite-V phase is the thermodynamically stable phase above 5 GPa. Therefore, “HP-ankerite” could be a potential metastable phase of ankerite. Its structure can be described in terms of trigonal planar ( $\text{CO}_3$ ) carbonate groups, sharing corners with ( $\text{FeO}_7$ ) pentagonal bipyramids and complex ( $\text{CaO}_9$ ) polyhedra. Note that the predicted transition pressure is lower than that reported in the literature for the spin crossover in siderite or magnesiosiderite iron-bearing carbonates [52].

Carbonates at depth could be strongly enriched in iron with respect to the surrounding minerals or carbonates at shallower depths. The implications of the present theoretical results would depend on the effects of high pressures in stabilizing a hypothetical ordered  $\text{CaFe}(\text{CO}_3)_2$  ankerite phase. Further experiments are needed in order to fully characterize the observed high-pressure  $\text{Ca}_{1.08(6)}\text{Mg}_{0.24(2)}\text{Fe}_{0.64(4)}\text{Mn}_{0.04(1)}(\text{CO}_3)_2$  polymorph, and confirm the existence of crystalline pure  $\text{CaFe}(\text{CO}_3)_2$  material at high pressures.

**Author Contributions:** Conceptualization, D.S.-P.; high-pressure XRD experiments, D.S.-P., J.R.-F., and C.P.; first-principle calculations, A.O.d.l.R.; formal analysis, R.C.-J. and D.S.-P.; writing, R.C.-J. and D.S.-P.; review, R.C.-J., D.S.-P., J.R.-F., A.O.d.l.R., and C.P. All authors have read and agreed to the published version of the manuscript.

**Funding:** This research was funded by the Spanish Ministerio de Ciencia, Innovación, y Universidades (MICINN) under the projects MALTA Consolider Ingenio 2010 network MAT2015-71070-REDC and PGC2018-097520-A-I00 (co-financed by EU FEDER funds), and by the Generalitat Valenciana under project PROMETEO/2018/123. D.S.-P. and A.O.R. acknowledge the financial support of the Spanish MINECO for the RyC-2014-15643 and RyC-2016-20301 Ramon y Cajal Grants, respectively. C.P. acknowledges the financial support of the Spanish Ministerio de Economía y Competitividad (MINECO project FIS2017-83295-P).

**Data Availability Statement:** Not applicable.

**Acknowledgments:** The authors thank Nicolescu and the Mineralogy and Meteoritics Department of the Yale Peabody Museum of Natural History for providing the mineral samples, and the ALBA-CELLS synchrotron for providing beamtime under experiment 2019093741. A.O.R. thanks the MALTA-Consolider supercomputing center and Compute Canada for computational resources.

**Conflicts of Interest:** The authors declare no conflict of interest.

## References

1. Zhang, J.; Martinez, I.; Guyot, F.; Reeder, R.J. Effects of Mg-Fe<sup>2+</sup> substitution in calcite-structure carbonates: Thermoelastic properties. *Am. Mineral.* **1998**, *83*, 280–287. [[CrossRef](#)]
2. Santamaria-Perez, D.; Garbarino, G.; Chulia-Jordan, R.; Dobrowolski, M.A.; Mühle, C.; Jansen, M. Pressure-induced transformations in mineral chalcocite, Cu<sub>2</sub>S, under hydrostatic conditions. *J. Alloys Compds.* **2014**, *610*, 645–650. [[CrossRef](#)]
3. Doll, K.; Schön, J.C.; Jansen, M. Global exploration of the energy landscape of solid on the ab initio level. *Phys. Chem. Chem. Phys.* **2007**, *9*, 6128–6133. [[CrossRef](#)] [[PubMed](#)]
4. Santamaria-Perez, D.; Thomson, A.; Segura, A.; Pellicer-Porres, J.; Manjon, F.J.; Cora, F.; McColl, K.; Wilson, M.; Dobson, D.; McMillan, P.F. Metastable structural transformations and pressure-induced amorphization in natural (Mg,Fe)<sub>2</sub>SiO<sub>4</sub> olivine under static compression: A Raman spectroscopic study. *Am. Mineral.* **2016**, *101*, 1642–1650. [[CrossRef](#)]
5. Dasgupta, R. Ingassing, storage, and outgassing of terrestrial carbon through geologic time. *Rev. Mineral. Geochem.* **2013**, *75*, 183. [[CrossRef](#)]
6. Zhang, J.; Reeder, R.J. Comparative compressibilities of calcite-structure carbonates: Deviations from empirical relations. *Am. Mineral.* **1999**, *84*, 861–870. [[CrossRef](#)]
7. Santamaria-Perez, D.; Otero-de-la-Roza, A.; Ruiz-Fuertes, J.; Chulia-Jordan, R.; Marqueño, T.; MacLeod, S.; Popescu, C. Pressure and temperature effects on low-density Mg<sub>3</sub>Ca(CO<sub>3</sub>)<sub>4</sub> huntite carbonate. *J. Phys. Chem. C* **2020**, *124*, 1077–1087. [[CrossRef](#)]
8. Chulia-Jordan, R.; Santamaria-Perez, D.; Otero-de-la-Roza, A.; Ruiz-Fuertes, J.; Marqueño, T.; Gomis, O.; MacLeod, S.; Popescu, C. Phase stability of natural Ni<sub>0.75</sub>Mg<sub>0.22</sub>Ca<sub>0.03</sub>CO<sub>3</sub> gaspeite mineral at high pressure and temperature. *J. Phys. Chem. C* **2020**, *124*, 19781–19792. [[CrossRef](#)]
9. Chulia-Jordan, R.; Santamaria-Perez, D.; Ruiz-Fuertes, J.; Otero-de-la-Roza, A.; Popescu, C. Crystal structure of BaCa(CO<sub>3</sub>)<sub>2</sub> alstonite carbonate and its phase stability upon compression. *ACS Earth Space Chem.* **2021**, *5*, 1130–1139. [[CrossRef](#)]
10. Ross, N.L.; Reeder, R.J. High-pressure structural study of dolomite and ankerite. *Am. Mineral.* **1992**, *77*, 412–421.
11. Santillán, J.; Williams, Q.; Knittle, E. Dolomite-II: A high-pressure polymorph of CaMg(CO<sub>3</sub>)<sub>2</sub>. *Geophys. Res. Lett.* **2003**, *30*, 1054. [[CrossRef](#)]
12. Solomatova, N.V.; Asimow, P.D. Ab initio study of the structure and stability of CaMg(CO<sub>3</sub>)<sub>2</sub> at high pressure. *Am. Mineral.* **2017**, *102*, 210–215. [[CrossRef](#)]
13. Zucchini, A.; Prencipe, M.; Belmonte, D.; Comodi, P. Ab initio study of the dolomite to dolomite-II high-pressure phase transition. *Eur. J. Mineral.* **2017**, *29*, 227–238. [[CrossRef](#)]
14. Solomatova, N.V.; Asimow, P.D. First-principles calculations of high-pressure iron-bearing monoclinic dolomite and single-cation carbonates with internally consistent Hubbard U. *Phys. Chem. Miner.* **2018**, *45*, 293–302. [[CrossRef](#)]
15. Boulard, E.; Menguy, N.; Auzende, A.L.; Benzerara, K.; Bureau, H.; Antonangeli, D.; Corgne, A.; Morard, G.; Siebert, J.; Perrillat, J.P.; et al. Experimental investigation of the stability of Fe-rich carbonates in the lower mantle. *J. Geophys. Res.* **2012**, *117*, B02208. [[CrossRef](#)]
16. Vennari, C.E.; Williams, Q. A novel carbon bonding environment in deep mantle high-pressure dolomite. *Am. Mineral.* **2018**, *103*, 171–174. [[CrossRef](#)]
17. Navrotsky, A.; Dooley, D.; Reeder, R.; Brady, P. Calorimetric studies of the energetics of the order-disorder in the system Mg<sub>1-x</sub>Fe<sub>x</sub>Ca(CO<sub>3</sub>)<sub>2</sub>. *Am. Mineral.* **1999**, *84*, 1622–1626. [[CrossRef](#)]
18. Tao, R.; Zhang, L.; Fei, Y.; Liu, Q. The effect of Fe on the stability of dolomite at high pressure: Experimental study and petrological observation in eclogite from southwestern Tianshan, China. *Geochim. Cosmochim. Acta.* **2014**, *143*, 253–267. [[CrossRef](#)]
19. Merlini, M.; Crichton, W.A.; Hanfland, M.; Gemmi, M.; Müller, H.; Kuppenko, I.; Dubrovinsky, L. Structures of dolomite at ultrahigh pressure and their influence on the deep carbon cycle. *PNAS* **2012**, *109*, 13509–13514. [[CrossRef](#)]
20. Efthimiopoulos, I.; Jahn, S.; Kuras, A.; Schade, U.; Koch-Müller, M. Combined high-pressure and high-temperature vibrational studies of dolomite: Phase diagram and evidence of a new distorted modification. *Phys. Chem. Miner.* **2017**, *44*, 465–476. [[CrossRef](#)]
21. Binck, J.; Chariton, S.; Stekiel, M.; Bayarjargal, L.; Morgenroth, W.; Millman, V.; Dubrovinsky, L.; Winkler, B. High-pressure, high-temperature phase stability of iron-poor dolomite and the structures of dolomite IIIc and dolomite-V. *Phys. Earth Planet. Int.* **2020**, *299*, 106403. [[CrossRef](#)]
22. Zhao, C.; Xu, L.; Gui, W.; Liu, J. Phase stability and vibrational properties of iron-bearing carbonates at high pressure. *Minerals* **2020**, *10*, 1142. [[CrossRef](#)]
23. Lippmann, F. Sedimentary Carbonate Minerals. In *Minerals, Rocks and Inorganic Materials*; Springer: Berlin/Heidelberg, Germany; New York, NY, USA, 1973.
24. Beran, A.; Zemann, J. Refinement and comparison of the crystal structures of a dolomite and of an Fe-rich ankerite. *TMPM Tschermaks Min. Petr. Mitt.* **1977**, *24*, 279–286. [[CrossRef](#)]
25. Davidson, P.M.; Symmes, G.H.; Cohen, B.A.; Reeder, R.J.; Lindsley, D.H. Synthesis of the new compound CaFe(CO<sub>3</sub>)<sub>2</sub> and experimental constraints on the (Ca,Fe)CO<sub>3</sub> join. *Geochim. Cosmochim. Acta* **1994**, *58*, 5105–5109. [[CrossRef](#)]
26. Fauth, F.; Peral, I.; Popescu, C.; Knapp, M. The new material science powder diffraction beamline at ALBA synchrotron. *Powder Diffr.* **2013**, *28*, S360. [[CrossRef](#)]

27. Chulia-Jordan, R.; Santamaria-Perez, D.; Marqueño, T.; Ruiz-Fuertes, J.; Daisenberger, D. Oxidation of high yield strength metals tungsten and rhenium in high-pressure high-temperature experiments of carbon dioxide and carbonates. *Crystals* **2019**, *9*, 676. [[CrossRef](#)]
28. Marqueño, T.; Santamaria-Perez, D.; Ruiz-Fuertes, J.; Chulia-Jordan, R.; Jorda, J.L.; Rey, F.; McGuire, C.; Kavner, A.; MacLeod, S.; Daisenberger, D.; et al. An ultrahigh CO<sub>2</sub>-loaded silicalite zeolite: Structural stability and physical properties at high pressures and temperatures. *Inorg. Chem.* **2018**, *57*, 6447–6455. [[CrossRef](#)]
29. Dewaele, A.; Loubeyre, P.; Mezouar, M. Equations of state of six metals above 94 GPa. *Phys. Rev. B Condens. Matter* **2004**, *70*, 094112. [[CrossRef](#)]
30. Klotz, S.; Chervin, J.C.; Munsch, P.; Le Marchand, G. Hydrostatic limits of 11 pressure transmitting media. *J. Phys. D Appl. Phys.* **2009**, *42*, 075413. [[CrossRef](#)]
31. Prescher, C.; Prakapenka, V.B. DIOPTAS: A program for reduction of two-dimensional x-ray diffraction data and data exploration. *High. Pressure Res.* **2015**, *35*, 223–230. [[CrossRef](#)]
32. Holland, T.J.B.; Redfern, S.A.T. Unit cell refinement from powder diffraction data: The use of regression diagnostics. *Mineral. Mag.* **1997**, *61*, 65–77. [[CrossRef](#)]
33. Nolze, G.; Kraus, W. Powdercell 2.0 for Windows. *Powd. Diffract.* **1998**, *13*, 256–259.
34. Blöchl, P.E. Projector augmented-wave method. *Phys. Rev. B* **1994**, *50*, 17953–17979. [[CrossRef](#)]
35. Giannozzi, P.; Andreussi, O.; Brumme, T.; Bunau, O.; Buongiorno Nardelli, M.; Calandra, M.; Car, C.; Cavazzoni, C.; Ceresoli, D.; Cococcioni, M.; et al. Advanced capabilities for materials modelling with Quantum ESPRESSO. *J. Phys. Condens. Matter.* **2017**, *29*, 465901. [[CrossRef](#)]
36. Dal Corso, A. Pseudopotentials periodic table: From H to Pu. *Comput. Mater. Sci.* **2014**, *95*, 337–350. [[CrossRef](#)]
37. Perdew, J.P.; Ruzsinszky, A.; Csonka, G.; Vydrov, O.A.; Scuseria, G.E.; Constantin, L.A.; Zhou, X.; Burke, K. Restoring the density-gradient expansion for exchange in solids and surface. *Phys. Rev. Lett.* **2008**, *100*, 136406. [[CrossRef](#)] [[PubMed](#)]
38. Marzari, N.; Vanderbilt, D.; de Vita, A.; Payne, M.C. Thermal contraction and disordering of the Al(110) surface. *Phys. Rev. Lett.* **1999**, *82*, 3296. [[CrossRef](#)]
39. Otero-De-La-Roza, A.; Luaña, V. Gibbs2: A new version of the quasi-harmonic model code. I. Robust treatment of the static data. *Comput. Phys. Commun.* **2011**, *182*, 1708–1720. [[CrossRef](#)]
40. Otero-De-La-Roza, A.; Abbasi-Pérez, D.; Luaña, V. Gibbs2: A new version of the quasiharmonic model code. II. Models for solid-state thermodynamics, features and implementation. *Comput. Phys. Commun.* **2011**, *182*, 2232–2248. [[CrossRef](#)]
41. Goldsmith, J.R.; Graf, D.L.; Witters, J.; Northrop, D.A. Studies in the system CaCO<sub>3</sub>-MgCO<sub>3</sub>-FeCO<sub>3</sub>. *J. Geol.* **1962**, *70*, 659–688. [[CrossRef](#)]
42. Giordano, V.M.; Datchi, F.; Gorelli, F.A.; Bini, R. Equation of state and anharmonicity of carbon dioxide phase I up to 12 GPa and 800 K. *J. Chem. Phys.* **2010**, *133*, 144501. [[CrossRef](#)] [[PubMed](#)]
43. Birch, F. Finite elastic strain of cubic crystals. *Phys. Rev.* **1947**, *71*, 809–824. [[CrossRef](#)]
44. Mao, Z.; Armentrout, M.; Rainey, E.; Manning, C.E.; Dera, P.; Prakapenka, V.B.; Kavner, A. Dolomite-III: A new candidate lower mantle carbonate. *Geophys. Res. Lett.* **2011**, *38*, 22303. [[CrossRef](#)]
45. Putz, H.; Schön, J.C.; Jansen, M. Combined method for “Ab Initio” structure solution from powder diffraction data. *J. Appl. Cryst.* **1999**, *32*, 864–870.42. [[CrossRef](#)]
46. Santamaria-Perez, D.; Haines, J.; Amador, U.; Morán, E.; Vegas, A. Structural characterization of a new high-pressure phase of GaAsO<sub>4</sub>. *Acta Cryst. B* **2006**, *62*, 1019–1024. [[CrossRef](#)]
47. Dinnebier, R.E.; Hinrichsen, B.; Lennie, A.; Jansen, M. High-pressure crystal structure of the non-linear optical compound BiB<sub>3</sub>O<sub>6</sub> from two-dimensional powder diffraction data. *Acta Cryst. B* **2009**, *65*, 1–10. [[CrossRef](#)]
48. Palaich, S.E.M.; Heffern, R.A.; Hanfland, M.; Lausi, A.; Kavner, A.; Manning, C.E.; Merlini, M. High-pressure compressibility and thermal expansion of aragonite. *Am. Mineral.* **2016**, *101*, 1651–1658. [[CrossRef](#)]
49. Bindi, L.; Roberts, A.C.; Biagioni, C. The crystal structure of alstonite, BaCa(CO<sub>3</sub>)<sub>2</sub>: An extraordinary example of ‘hidden’ complex twinning in large single crystals. *Miner. Magaz.* **2020**, *84*, 699–704. [[CrossRef](#)]
50. Santamaria-Perez, D.; Ruiz-Fuertes, J.; Marqueño, T.; Pellicer-Porres, J.; Chulia-Jordan, R.; MacLeod, S.; Popescu, C. Structural behavior of natural silicate-carbonate spurrite mineral, Ca<sub>5</sub>(SiO<sub>4</sub>)<sub>2</sub>(CO<sub>3</sub>), under high-pressure, high-temperature conditions. *Inorg. Chem.* **2018**, *57*, 98–105. [[CrossRef](#)] [[PubMed](#)]
51. Santamaria-Perez, D.; Ruiz-Fuertes, J.; Peña-Alvarez, M.; Chulia-Jordan, R.; Marqueño, T.; Zimmer, D.; Gutierrez-Cano, V.; MacLeod, S.; Gregoryanz, E.; Popescu, C.; et al. Post-tillelyite, a dense calcium silicate-carbonate phase. *Sci. Rep.* **2019**, *9*, 7898. [[CrossRef](#)] [[PubMed](#)]
52. Weis, C.; Sternemann, C.; Cerantola, V.; Sahle, C.J.; Spiekermann, G.; Harder, M.; Forov, Y.; Kononov, A.; Sakrowski, R.; Yavas, H.; et al. Pressure driven spin transition in siderite and magnesiosiderite single crystals. *Sci. Rep.* **2017**, *7*, 16526. [[CrossRef](#)] [[PubMed](#)]